

One-dimensional electronic states in a natural misfit structure

Alla Chikina,¹ Gargee Bhattacharyya,² Davide Curcio,¹ Charlotte E. Sanders,³ Marco Bianchi,¹ Nicola Lanatà,^{2,4} Matthew Watson,⁵ Cephise Cacho,⁵ Martin Bremholm,⁶ and Philip Hofmann^{1,*}

¹*Department of Physics and Astronomy, Interdisciplinary Nanoscience Center (iNANO), Aarhus University, 8000 Aarhus C, Denmark*

²*Department of Physics and Astronomy, Aarhus University, 8000, Aarhus C, Denmark*

³*Central Laser Facility, STFC Rutherford Appleton Laboratory, Harwell OX11 0QX, United Kingdom*

⁴*Nordita, KTH Royal Institute of Technology and Stockholm University, Roslagstullsbacken 23, 10691 Stockholm, Sweden*

⁵*Diamond Light Source, Division of Science, Didcot, United Kingdom*

⁶*Department of Chemistry, Interdisciplinary Nanoscience Center (iNANO), Aarhus University, 8000 Aarhus C, Denmark*
(Dated: May 12, 2022)

Misfit compounds are thermodynamically stable stacks of two-dimensional materials, forming a three-dimensional structure that remains incommensurate in one direction parallel to the layers. As a consequence, no true bonding is expected between the layers, with their interaction being dominated by charge transfer. In contrast to this well-established picture, we show that interlayer coupling can strongly influence the electronic properties of one type of layer in a misfit structure, in a similar way to the creation of modified band structures in an artificial moiré structure between two-dimensional materials. Using angle-resolved photoemission spectroscopy with a micron-scale light focus, we selectively probe the electronic properties of hexagonal NbSe₂ and square BiSe layers that terminate the surface of the (BiSe)_{1+δ}NbSe₂ misfit compound. We show that the band structure in the BiSe layers is strongly affected by the presence of the hexagonal NbSe₂ layers, leading to quasi one-dimensional electronic features. The electronic structure of the NbSe₂ layers, on the other hand, is hardly influenced by the presence of the BiSe. Using density functional theory calculations of the unfolded band structures, we argue that the preferred modification of one type of bands is mainly due to the atomic and orbital character of the states involved, opening a promising way to design novel electronic states that exploit the partially incommensurate character of the misfit compounds.

A stack of two-dimensional (2D) materials bound by van der Waals forces is naively not expected to show strong interlayer interactions, aside from a possible charge transfer, especially when the two crystal lattices do not have the same unit cell or orientation [1]. However, precisely systems of this category have shown extremely rich physics caused by the formation of moiré lattices, band replicas and flat bands [2–5], or even merely by the relative position of high symmetry points that can strongly affect the stack’s excitonic properties [6].

A similar situation could be expected in the so-called misfit compounds [7, 8]. These are stacks of alternating 2D square and hexagonal lattices that result in a structure which is commensurate in one direction but incommensurate along the perpendicular direction in the plane of the 2D layers (see Figure 1(a)). The lack of commensurability prevents the formation of interlayer chemical bonds, but charge transfer between the layers can be substantial and can help to stabilize the misfit compounds [9–11]. An electronic interlayer interaction beyond charge transfer has so far not been reported. However, it is well known that the two layers are affected by each other’s presence such that the lattice structure of each layer is modulated by the periodicity of the other layer [7, 12], something that ought to be manifest also in the electronic structure. One might ask whether misfit crystals can exhibit phenomena analogous to, e.g., twisted bilayer graphene. However, the misfit compounds are different from most of the artificial stacks of 2D materials studied

so far [13–15] in the sense that the latter usually combine two hexagonal lattices, whereas a misfit structure consists of hexagonal and square lattices.

Here we study the (BiSe)_{1+δ}NbSe₂ misfit compound. The structure shown in Figure 1(a) is a stack of square BiSe layers and hexagonal NbSe₂ layers (slightly deformed such that there is commensurability in the y direction). Based on transport data, charge transfer is not expected to play a major role in this compound [9, 16]. The material is superconducting with a T_c around 2.5 K, and an argument has been made that the superconductivity does not have the 2D character of a NbSe₂ intercalation compound but is rather of a three-dimensional nature [17]. We characterise the samples using angle-resolved photoemission spectroscopy (ARPES) with a small light focus, giving us the possibility to individually probe the electronic structure of different surface terminations (by BiSe or NbSe₂ layers) and thereby to draw conclusions about the misfit structure’s effect on the individual layers. The experimental findings suggest a hitherto unobserved interlayer interaction, leading to the emergence of one-dimensional features in the electronic structure. They are supported by density functional theory (DFT) calculations.

(BiSe)_{1+δ}NbSe₂ misfit crystals were grown following the procedure given by Nagao *et al.* [18], using a nominal $\delta = 0.4$. Conventional ARPES experiments were performed at the SGM-3 beamline of ASTRID2 [19] and small-spot (microARPES) measurements were carried

out at the I05 beamline of Diamond Light Source (DLS). The light spot size was on the order of $200 / 5 \mu\text{m}$ at ASTRID2 / DLS. The sample temperature was $45 / 55 \text{ K}$; energy and angular resolution were $35 / 30 \text{ meV}$ and 0.2° . The photon energy is given in the figures. Electronic structure calculations for individual BiSe and NbSe₂ layers as well as for a commensurate approximation to the misfit structure were performed using the Vienna *Ab initio* Simulation Package (VASP) [20, 21]. Unfolding calculations were performed using the new patch version of VASP (UnfoldingPatch4vasp) and b4vasp packages [22]. Details about structural relaxation and the band structure unfolding are given in the Appendix.

The misfit structure shown in Figure 1(a) is preferentially cleaved between the 2D layers, resulting in a surface that is either terminated by NbSe₂ or by BiSe, as shown Fig. 1(b) and (c). Due to the surface sensitivity of ARPES, the photoemission intensity is expected to be dominated by the topmost layer. However, when a sufficiently large surface area is probed, both terminations are expected to be present in equal amounts. Figure 1(c) shows the photoemission intensity at the Fermi level E_F , obtained using a large UV light spot ($\approx 100 \times 190 \mu\text{m}^2$), presumably averaging over the two different surface terminations. The result strongly resembles ARPES results from NbSe₂ [23–28], with the characteristic hole pockets around the Γ and K points of the hexagonal Brillouin zone (BZ). Superficially, no distinct features obviously stemming from the BiSe layers are visible. While surprising, this is consistent with recent ARPES studies of similar misfit compounds that did not reveal *any* sign of the cubic layers’ electronic structure [10, 11]. However, upon closer inspection, we note that the hexagonal hole pocket around Γ_1 appears “filled” and thereby distinctly different from the one in the neighbouring BZ around Γ_2 and from that expected for NbSe₂ [23]. As we shall see below, this is in fact a contribution of the BiSe layers.

From the size of the NbSe₂ Fermi contour, we can determine an additional band filling of 0.26 ± 0.01 electrons per NbSe₂ unit cell compared to the charge-neutral single-layer (see Appendix). This is consistent with a charge transfer between the layers and with a relative shift of the bands in the calculated electronic structure of the misfit approximant; see Appendix. Note, however, that without an independent measurement of the BiSe Fermi contour, it is not possible to disentangle a charge transfer between the layers from a possible overall doping of the sample, something that could arise from the formation of non-stoichiometric defects [29].

A more detailed insight into the termination-dependent electronic structure is gained by scanning a highly focused ($\approx 5 \mu\text{m}$) UV beam across the surface, such that regions with a unique surface termination are resolved (see Figure 2(a,b)). When performing such a scan over an area of $43 \times 40 \mu\text{m}^2$, we find the electronic structure to be dominated by the two types of dispersion

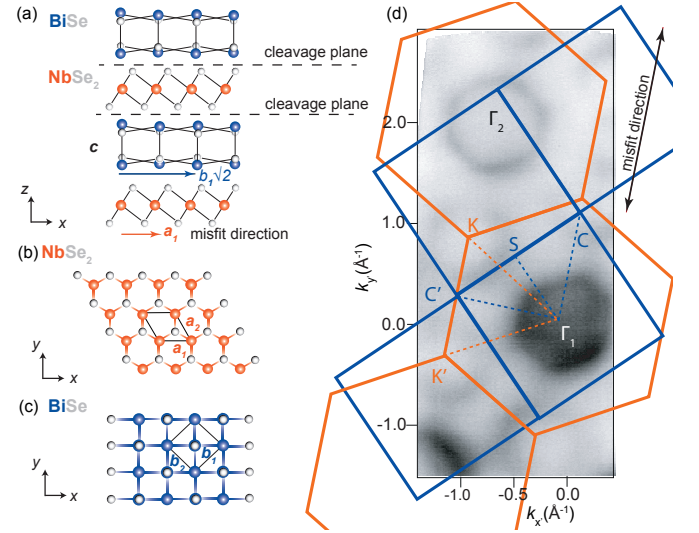


FIG. 1: (Color online) (a) Side-view of the $(\text{BiSe})_{1+\delta}\text{NbSe}_2$ misfit compound. Dashed lines indicate possible cleavage planes. The incommensurate direction is labelled as “misfit direction”. (b) and (c) Top view of the structure’s NbSe₂ and BiSe layers with the unit cells indicated. (d) Photoemission intensity at the Fermi energy (high intensity is dark) taken at 65eV photon energy with the 2D Brillouin zones for square BiSe and hexagonal NbSe₂ superimposed. The corners of the BiSe Brillouin zone are called C and C’ to account for the broken symmetry.

shown in Figure 2(c) and (d), which we ascribe to the two surface terminations (NbSe₂ and BiSe). Assigning the type of termination is achieved by a comparison to DFT calculations for isolated single-layers of NbSe₂ and BiSe (Figures 2(e) and (f), respectively) (see Appendix). The electronic structure of the two layers is sufficiently different for this to be straight-forward: For NbSe₂, the Γ point is encircled by a hole pocket as shown in Figure 2(c) and (e) (marked by green arrows). BiSe also shows a hole pocket around Γ but with the simultaneous presence of an occupied electron-like band, as seen in Figure 2(d) and (f) (the bands giving rise to the hole pocket are also marked in panel (f)). Since ARPES does not exclusively probe the first layer and since the spatial resolution is limited, the electron band is also faintly visible for the NbSe₂ termination, but it is much weaker. Figure 2(b) shows the photoemission intensity in a region of interest around this electron band, marked by a rectangle in Figure 2(d), and high intensity therefore indicates the presence of the BiSe termination. The clear distinction between the two surface terminations is also supported by mapping their qualitatively different core level spectra, as discussed in the Appendix.

While a detailed inspection of the NbSe₂-terminated regions gives results that are very similar to bulk NbSe₂ crystals or single-layers, apart from the aforementioned strong doping effects [23–28] (see Appendix), the results from the BiSe-terminated parts are more complex. The

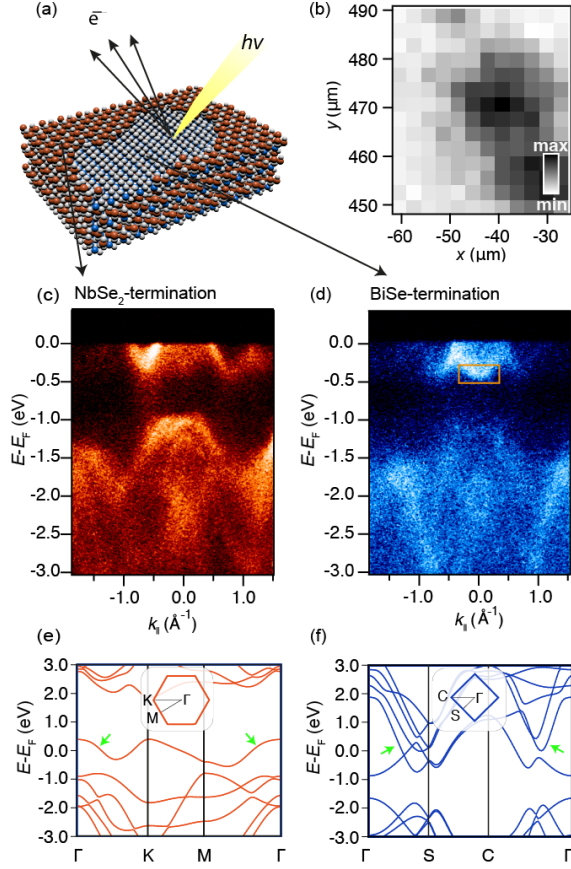


FIG. 2: (a) Sketch of the experimental geometry. A highly focused UV beam is scanned across the surface of the misfit compound, leading to photoemission from only one of the two possible terminations of the crystal. (b) Map of the (x, y) -dependent photoemission intensity integrated over the rectangular region of interest in panel (d). (c,d) Distinctly different spectra collected at 133 eV photon energy from NbSe₂ and BiSe surface terminations. (e,f) Calculated electronic structure for an isolated 2D layer of NbSe₂ and BiSe, respectively. The 2D BZs are shown as insets. The green arrows mark the bands leading to hole pockets around Γ .

photoemission intensity at E_F , as well as along cuts throughout the 2D square BZ, is shown in Figure 3(a) and (b), respectively. The characteristic features of the NbSe₂ termination are still dominating. However, and in contrast to the results of Refs. [10, 11], we also find photoemission features that do not originate from the NbSe₂ layers, such as the aforementioned electron band around the Γ -point. It has a similar dispersion as in the calculation of Figure 2(f) but it is less occupied, also supporting a charge transfer from BiSe to NbSe₂. Moreover, this dispersion is smeared out in all directions, explaining the “filled” character of the Fermi contour around Γ . Further out towards the BZ boundary, there is a downward dispersing band forming a hole-like Fermi contour, also in good agreement with the calculation, see arrows in Figure 2(f). Due to the simultaneously present photoe-

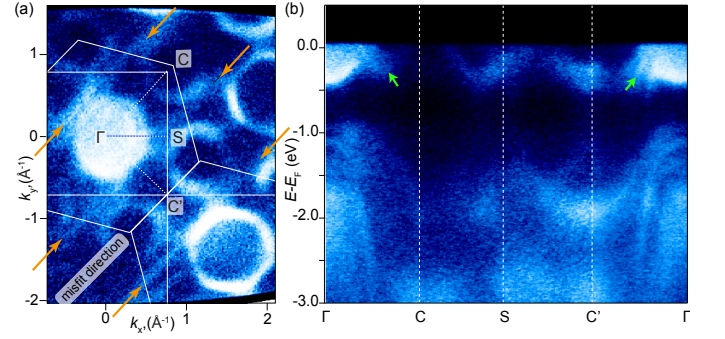


FIG. 3: (a) Photoemission intensity at the Fermi level recorded at 133 eV photon energy for the BiSe termination. The orange arrows mark one-dimensional lines of high photoemission intensity in the misfit direction. (b) Dispersion in the square Brillouin zone of BiSe. The green arrows mark the dispersion from two hole pockets, one from BiSe and one from NbSe₂.

mission intensity from the NbSe₂, what is observed are actually two superimposed hole pockets, seen near the arrows in Fig. 3(b) and in more detail in the Appendix. No replicas of the electron band can be found around higher reciprocal lattice vectors of the square BiSe lattice.

The most interesting features observed on the BiSe termination are one-dimensional (1D) lines of strong photoemission intensity at E_F (marked by arrows in Figure 3(a)). Similar structures also appear at higher binding energies and we can exploit their 1D nature to identify the incommensurate (misfit) direction (see Appendix). The 1D lines resemble those typically found for nearly 1D materials [30] and they do not appear in any of the misfit structure’s constituent layers on their own, so evidently they manifest a hitherto unseen interlayer interaction that goes beyond charge transfer.

A plausible explanation for these observations arises from the structural interaction between the 2D materials in the misfit compound, as well as from the orbital character of the bands near E_F . The interaction between the 2D sheets causes each to be distorted in a nonperiodic fashion. In a misfit crystal of composition MX TX₂, the modulation-induced deformation is typically highest for the atoms at the interface, i.e., the entire MX layer and the X atoms from TX₂, while the T atoms in the TX₂ layers are least affected [7, 12, 31, 32]. This explains why the NbSe₂ Fermi contour, which is formed from Nb 3d orbitals, is hardly influenced by the formation of the misfit compound. Interestingly, even the deeper lying Se-derived bands around 1 eV below E_F are still very similar to those in single-layer NbSe₂ [33], suggesting that the entire NbSe₂ layer is little affected by the presence of the BiSe. The BiSe states near E_F , on the other hand, have Bi 6p character (see Appendix) and are therefore susceptible to the changed electronic environment of the Bi atoms, as well as to the loss of periodicity in the misfit

direction. The resulting electronic structure of BiSe near E_F will thus no longer be periodic in the misfit direction. These considerations can explain the absence of a periodicity following the square BiSe reciprocal lattice and the emergence of a 1D electronic structure.

We support these arguments by DFT calculations. In order to understand the formation of the 1D structures at E_F , we start by inspecting the Fermi contours for free-standing layers of NbSe₂ and BiSe, with the lattice parameters constrained to the value found for the misfit approximant. The superposition of the two contours is shown in Figure 4(a). It would represent the Fermi contour of the misfit compound in the absence of any interlayer interaction and charge transfer, with each Fermi contour repeated according to its reciprocal lattice. Clearly, this is not supported by the experiment. For a more appropriate description, and given the experimental evidence of a hardly affected NbSe₂ band structure, we start to approximate the misfit structure by a rigid NbSe₂ layer and ask how its periodic potential affects the electronic structure of the neighbouring BiSe layers or the electronic structure of the combined misfit crystal. To this end, we calculate the electronic structure of a NbSe₂ and a BiSe layer, as well as a (BiSe)_{1.14}NbSe₂ misfit approximant in a commensurate unit cell of 7 NbSe₂ and $8/\sqrt{2}$ BiSe lattice vectors along the misfit direction. We then unfold the electronic structure calculated in this supercell onto the primitive unit cell of NbSe₂ — see Appendix.

The spectral functions near the Fermi energy resulting from the band unfolding (for a definition see Appendix) are given in Figure 4(b)-(d). For a large supercell just containing NbSe₂, the unfolding on the primitive cell in Figure 4(b) merely gives the expected Fermi contour of this layer. For a single layer of BiSe and for the misfit approximant, the result is more complex (see Figure 4(c),(d)) but in both cases, one can readily make out 1D features along the misfit direction, similar to those observed in the experiment. This is especially pronounced for the unfolded electronic bands of the misfit approximant (marked by arrows). The origin of the 1D structure is a complex interplay of lost translational symmetry and interlayer interaction. The original electronic structure elements responsible for the lines are the straight sides of the hexagonal hole pocket around Γ for NbSe₂, as well as the almost straight lines of the electron / hole pockets in BiSe. These two features are not simply superimposed. They interact strongly, as can be seen by comparing the unfolded band structure of the misfit approximant with those of the individual single layers, and as is also plausible considering their predominant orbital character (Bi p_z and Nb d_{z^2}).

The basic assumption of the calculations is a fairly rigid NbSe₂ template, imposing its structure onto the BiSe layer and thereby justifying the choice of projecting the bands onto the NbSe₂ lattice. This is based on struc-

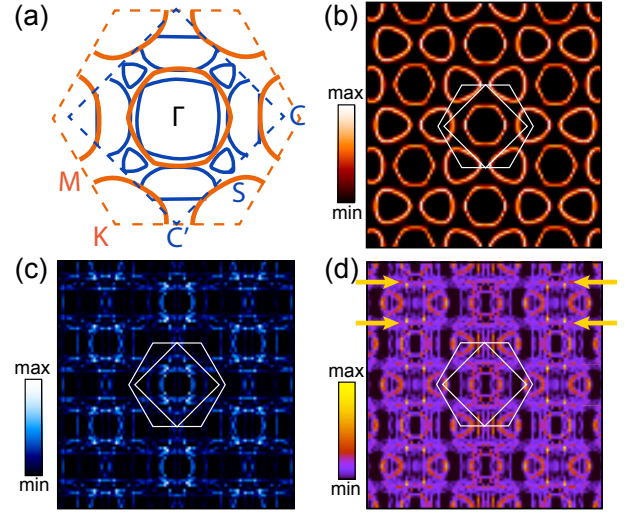


FIG. 4: (a) Calculated Fermi contour for free-standing NbSe₂ and BiSe layers, using the experimentally determined Fermi level. (b) Spectral function near E_F for NbSe₂ in the approximate unit cell of the misfit structure, unfolded onto the primitive NbSe₂ reciprocal lattice. (c) and (d) Corresponding spectral functions unfolded on the primitive NbSe₂ lattice for free-standing BiSe and the complete misfit structure. The arrows mark the position of one-dimensional features in the electronic structure.

tural arguments and on the finding from ARPES that the NbSe₂ band structure is almost unaffected by the presence of BiSe, apart from charge transfer. This view is not only supported by the formation of the 1D structures but also by the continuous presence of the NbSe₂ hole pockets around the K points in Figure 4(d). These pockets are placed in an area where there are few BiSe states available for hybridization and they are thus unaffected by the misfit structure, merely shrinking a little due to the charge transfer. Note that the full effect of the incommensurate structure can, of course, not be captured in a periodic calculation with a large but commensurate unit cell, nor can additional factors that could lead to a 1D behaviour, such as the possible formation of Bi antiphase domain boundaries [34]. These restrictions can explain why the measured 1D lines appear even more uniform than in the calculation.

The misfit-induced transition from a 2D electronic structure to a 1D situation in the BiSe layers could have several interesting consequences. By definition, it effectively localizes the electrons in the incommensurate direction, preventing metallic transport through the BiSe layer in that direction. This is consistent with earlier findings in transport experiments, where an electron localization due to the incommensurate potential has been invoked to explain the fact that only the TS₂ layers contribute to the electric conductivity of some rare earth-based misfit compounds [35–37]. The creation of the 1D Fermi contour could further give rise to the rich physics

expected in such situations, potentially giving rise to Peierls distortions, spin-charge separation or the formation of Luttinger liquid states.

In summary, we have shown that the incommensurate interlayer interaction in the $(\text{BiSe})_{1+\delta}\text{NbSe}_2$ misfit compound leads to a dimensionality reduction of the electronic structure in the square BiSe lattice, from a 2D to a 1D metallic state. This can explain earlier transport experiments in this class of materials that have found conductivity to be located exclusively in the transition metal dichalcogenide layer. It opens the possibility to realize 1D physics in this class of naturally occurring stacks of layered materials, exploiting the design freedom where doping, charge transfer and the mechanical properties of the constituent layers can be widely tuned.

This work was supported by VILLUM FONDEN via the Centre of Excellence for Dirac Materials (Grant No. 11744) and the Independent Research Fund Denmark (Grant No. 1026-00089B). We acknowledge Diamond Light Source for time on Beamline I05 under Proposal SI25201-2. We thank Richard Balog, Kimberly Hsieh and Jeppe Vang Lauritzen for discussions and technical support.

APPENDIX

Termination-dependent ARPES results

Identifying the two surface terminations (BiSe and NbSe_2) is easily achieved by their characteristic ARPES spectra, as demonstrated in the main text. For the data shown in the main text, the light spot is moved across the surface and the local photoemission intensity is measured as a function of energy and angle. Since the sample is not necessarily well-aligned with the scanning grid, the ARPES spectra do not represent cuts along a particular high symmetry direction in the Brillouin zone. Figure 5 shows that the position-resolved local core level spectra can also be used for the purpose of distinguishing the surface terminations. Figure 5(a) and (b) reproduce the result from Figure 2 in the main text. Figure 5(c), (d) and (e), (f) show corresponding results for the Se 3d and Bi 5d core level spectra, respectively. The maps are generated by integrating the core level spectra between the dashed lines. The largest differences between the terminations are found in the Se 3d core level spectrum which shows four distinct peaks for the NbSe_2 terminations but only two for the BiSe termination (there are, of course, always contributions from the other layer / termination present as well). The relative photoemission intensity of the Bi 5d spectra is also consistent the termination assignment, with the blue spectrum from the BiSe termination always being higher in intensity than the the orange spectrum from the NbSe_2 termination. The three intensity maps agree well with each other (apart from the

expected contrast reversal in panel (c)), confirming the consistency of the termination assignment between the different approaches.

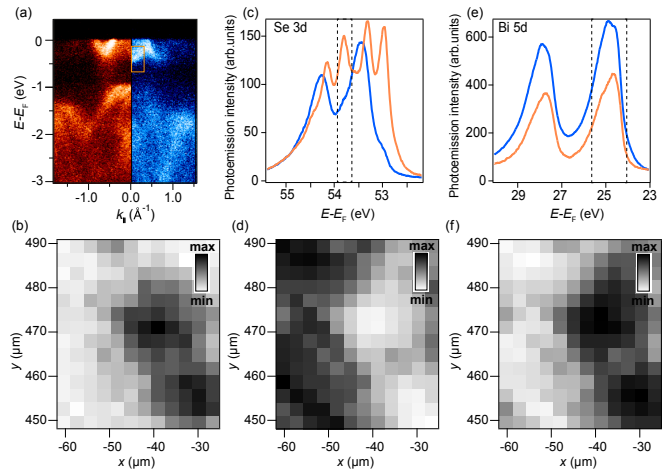


FIG. 5: (a) and (b) Reproduction of the data in Figure 2 of the main text. (c) Se 3d core level spectra taken at 133 eV photon energy for the BiSe and NbSe_2 termination in blue and orange, respectively. (d) Integrated intensity in the energy range between the dashed lines in panel (c). (e) and (f) Corresponding result for Bi 5d.

Figure 6 shows the photoemission at E_F and along the high symmetry directions of the Brillouin zone (BZ) for the NbSe_2 termination, i.e. the result corresponding to Figure 3 of the main text.

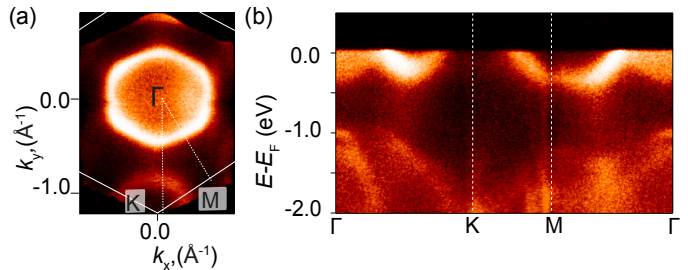


FIG. 6: (a) Photoemission intensity at the Fermi level taken at 65 eV photon energy for the NbSe_2 termination. (b) Dispersion throughout the hexagonal Brillouin zone of NbSe_2 .

The one-dimensional (1D) features in the electronic structure of the BiSe termination do not only appear at the Fermi energy. Figure 7(a)-(f) illustrates this for higher binding energies. We can use these 1D features to find the incommensurate misfit direction using two different arguments. First, the loss of periodicity in the misfit direction implies that k in the misfit direction is no longer a meaningful quantum number. In the most extreme case, a complete collapse of k -space would occur in this direction, similar to a crystal truncation rod in X-ray diffraction. Smearing out of features must thus

occur in the misfit direction. A second argument can be based on the symmetry of the electronic structure. Due to the alignment of the NbSe₂ and BiSe layers, the misfit direction must coincide with $\Gamma-K$ direction of the hexagonal Brillouin zone of NbSe₂. This means that the misfit direction must either coincide with the 1D features, or it must be at an angle of 60° with this direction. The latter possibility cannot be reconciled with the overall symmetry of the system.

Having identified the misfit direction in the data collected with a small light spot at DLS, we can use the maps collected at higher binding energy to find the misfit direction in the data from ASTRID2, despite of the absence of clear 1D features at E_F . Particularly useful structures for this purpose stem from the electron band at Γ at energies of 200 - 300 meV below E_F .

Figure 7(g)-(j) provides additional data for the electronic structure around the Γ_1 point, illustrating the simultaneous presence of two hole pockets around Γ , one from BiSe and one from NbSe₂. This is best seen in the cuts shown in panels (h) and (j).

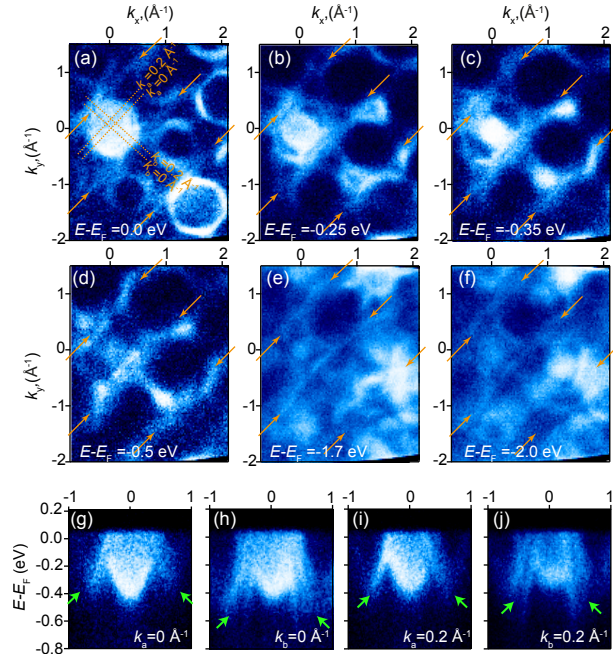


FIG. 7: (a) - (f) Photoemission intensity maps at constant binding energy taken at 133 eV photon energy for the BiSe termination of the misfit crystal. The 1D features can be seen at different binding energies and are marked by arrows. (g) - (j) Photoemission intensity as a function of energy and k_{\parallel} for the paths marked in panel (a) showing the electron band and additional hole pocket dispersions (the hole pockets are marked by green arrows).

Theory Details

The density functional theory calculations were performed using the Vienna *Ab initio* Simulation Package (VASP) [20, 21]. The electron-electron exchange and correlation potentials were described using the generalized gradient approximation Perdew-Burke-Ernzerhof functional [38, 39]. The plane wave energy cutoff was set to 500 eV. The van der Waals corrected density functional proposed by Grimme was used for treating the dispersion interactions [40]. A vacuum region of 15 Å was set along the z -direction, for avoiding spurious interactions between the periodic repetitions of the monolayer NbSe₂ and BiSe systems. A Γ -centered \mathbf{k} -point grid of $1 \times 4 \times 1$ was used to sample the first BZ of the misfit structure, both for the geometry optimization and for the band-structure calculations.

The single-layer band structures for NbSe₂ and BiSe in Figure 2 of the main text were obtained after performing a constrained relaxation assuming exact hexagonal and square structures, respectively. The resulting primitive-cell parameters were $a_1 = a_2 = 3.45$ Å for NbSe₂ (see Figure 1(b) of the main text), while they were $b_1 = b_2 = 4.25$ Å for BiSe (see Figure 1(c) of the main text). The misfit structure was fully optimized assuming the approximate commensurate superstructure shown in Figure 8. The size of the superstructure is $a = 24.25$ Å, $b = 5.97$ Å, and $c = 24.16$ Å, along the x , y and z directions, respectively. The resulting atomic positions in this supercell are reported in Table I.

Table I : Relaxed atomic positions of misfit structure in Å.

Atom	x	y	z
Nb ₁	6.06	3.44	6.04
Nb ₂	18.19	3.44	18.12
Nb ₃	18.19	0.46	6.04
Nb ₄	6.06	0.46	18.12
Nb ₅	0.87	0.48	6.05
Nb ₆	23.37	0.48	18.10
Nb ₇	23.37	3.46	6.05
Nb ₈	0.87	3.46	18.10
Nb ₉	13.00	0.48	18.13
Nb ₁₀	11.24	0.48	6.02

Atom	x	y	z	Atom	x	y	z
Nb ₁₁	11.24	3.46	18.13	Se ₁₃	16.45	4.46	19.76
Nb ₁₂	13.00	3.46	6.02	Se ₁₄	7.79	4.46	4.39
Nb ₁₃	14.71	0.46	6.05	Se ₁₅	7.79	1.48	19.76
Nb ₁₄	9.53	0.46	18.10	Se ₁₆	16.45	1.48	4.39
Nb ₁₅	9.53	3.45	6.05	Se ₁₇	14.73	4.43	7.73
Nb ₁₆	14.71	3.45	18.10	Se ₁₈	9.51	4.43	16.42
Nb ₁₇	2.58	0.46	18.13	Se ₁₉	9.51	1.45	7.73
Nb ₁₈	21.66	0.46	6.02	Se ₂₀	14.73	1.45	16.42
Nb ₁₉	21.66	3.45	18.13	Se ₂₁	2.61	4.43	19.81
Nb ₂₀	2.58	3.45	6.02	Se ₂₂	21.64	4.43	4.34
Nb ₂₁	4.33	0.49	6.02	Se ₂₃	21.64	1.45	19.81
Nb ₂₂	19.91	0.49	18.13	Se ₂₄	2.61	1.45	4.34
Nb ₂₃	19.91	3.47	6.02	Se ₂₅	11.26	4.46	7.70
Nb ₂₄	4.33	3.47	18.13	Se ₂₆	12.98	4.46	16.45
Nb ₂₅	16.46	0.49	18.10	Se ₂₇	12.98	1.48	7.70
Nb ₂₆	7.79	0.49	6.05	Se ₂₈	11.26	1.48	16.45
Nb ₂₇	7.79	3.47	18.10	Se ₂₉	23.39	4.46	19.78
Nb ₂₈	16.46	3.47	6.05	Se ₃₀	0.86	4.46	4.37
Se ₁	0.85	4.43	7.71	Se ₃₁	0.86	1.48	19.78
Se ₂	23.39	4.43	16.44	Se ₃₂	23.39	1.48	4.37
Se ₃	23.39	1.45	7.71	Se ₃₃	7.79	4.44	7.70
Se ₄	0.85	1.45	16.44	Se ₃₄	16.45	4.44	16.45
Se ₅	12.98	4.43	19.79	Se ₃₅	16.45	1.45	7.70
Se ₆	11.26	4.43	4.36	Se ₃₆	7.79	1.45	16.45
Se ₇	11.26	1.45	19.79	Se ₃₇	19.92	4.44	19.78
Se ₈	12.98	1.45	4.36	Se ₃₈	4.32	4.44	4.37
Se ₉	4.32	4.46	7.68	Se ₃₉	4.32	1.45	19.78
Se ₁₀	19.92	4.46	16.47	Se ₄₀	19.92	1.45	4.37
Se ₁₁	19.92	1.48	7.68	Se ₄₁	21.65	4.45	7.72
Se ₁₂	4.32	1.48	16.47	Se ₄₂	2.59	4.45	16.43

Atom	x	y	z	Atom	x	y	z
Se ₄₃	2.59	1.47	7.72	Se ₇₃	19.70	2.95	13.28
Se ₄₄	21.65	1.47	16.43	Se ₇₄	4.55	2.95	10.88
Se ₄₅	9.53	4.45	19.80	Se ₇₅	4.55	5.93	13.28
Se ₄₆	14.72	4.45	4.35	Se ₇₆	19.70	5.93	10.88
Se ₄₇	14.72	1.47	19.80	Se ₇₇	7.57	2.95	1.19
Se ₄₈	9.53	1.47	4.35	Se ₇₈	16.68	2.95	22.96
Se ₄₉	18.17	4.44	7.73	Se ₇₉	16.68	5.93	1.19
Se ₅₀	6.07	4.44	16.42	Se ₈₀	7.57	5.93	22.96
Se ₅₁	6.07	1.46	7.73	Se ₈₁	1.50	2.94	13.29
Se ₅₂	18.17	1.46	16.42	Se ₈₂	22.74	2.94	10.86
Se ₅₃	6.05	4.44	19.81	Se ₈₃	22.74	5.93	13.29
Se ₅₄	18.20	4.44	4.34	Se ₈₄	1.50	5.93	10.86
Se ₅₅	18.20	1.46	19.81	Se ₈₅	13.63	2.94	1.21
Se ₅₆	6.05	1.46	4.34	Se ₈₆	10.62	2.94	22.94
Se ₅₇	7.58	2.92	13.28	Se ₈₇	10.62	5.93	1.21
Se ₅₈	16.66	2.92	10.87	Se ₈₈	13.63	5.93	22.94
Se ₅₉	16.66	5.91	13.28	Bi ₁	7.57	5.87	13.76
Se ₆₀	7.58	5.91	10.87	Bi ₂	16.67	5.87	10.39
Se ₆₁	19.71	2.92	1.20	Bi ₃	16.67	2.89	13.76
Se ₆₂	4.53	2.92	22.95	Bi ₄	7.57	2.89	10.39
Se ₆₃	4.53	5.91	1.20	Bi ₅	19.70	5.87	1.68
Se ₆₄	19.71	5.91	22.95	Bi ₆	4.54	5.87	22.47
Se ₆₅	13.65	2.94	13.28	Bi ₇	4.54	2.89	1.68
Se ₆₆	10.60	2.94	10.87	Bi ₈	19.70	2.89	22.47
Se ₆₇	10.60	5.92	13.28	Bi ₉	13.65	5.87	13.76
Se ₆₈	13.65	5.92	10.87	Bi ₁₀	10.60	5.87	10.39
Se ₆₉	1.52	2.94	1.20	Bi ₁₁	10.60	2.89	13.76
Se ₇₀	22.72	2.94	22.95	Bi ₁₂	13.65	2.89	10.39
Se ₇₁	22.72	5.92	1.20	Bi ₁₃	1.52	5.87	1.68
Se ₇₂	1.52	5.92	22.95	Bi ₁₄	22.72	5.87	22.47

Atom	x	y	z
Bi ₁₅	22.72	2.89	1.68
Bi ₁₆	1.52	2.89	22.47
Bi ₁₇	19.70	5.86	13.78
Bi ₁₈	4.55	5.86	10.38
Bi ₁₉	4.55	2.87	13.78
Bi ₂₀	19.70	2.87	10.38
Bi ₂₁	7.57	5.86	1.70
Bi ₂₂	16.67	5.86	22.46
Bi ₂₃	16.67	2.87	1.70
Bi ₂₄	7.57	2.87	22.46
Bi ₂₅	1.51	5.88	13.76
Bi ₂₆	22.73	5.88	10.39
Bi ₂₇	22.73	2.90	13.76
Bi ₂₈	1.51	2.90	10.39
Bi ₂₉	13.64	5.88	1.68
Bi ₃₀	10.61	5.88	22.47
Bi ₃₁	10.61	2.90	1.68
Bi ₃₂	13.64	2.90	22.47

Note that these relaxed positions correspond to structural distortions of ~ 0.05 Å for NbSe₂ and BiSe, with respect to their respective individually-relaxed free-standing values.

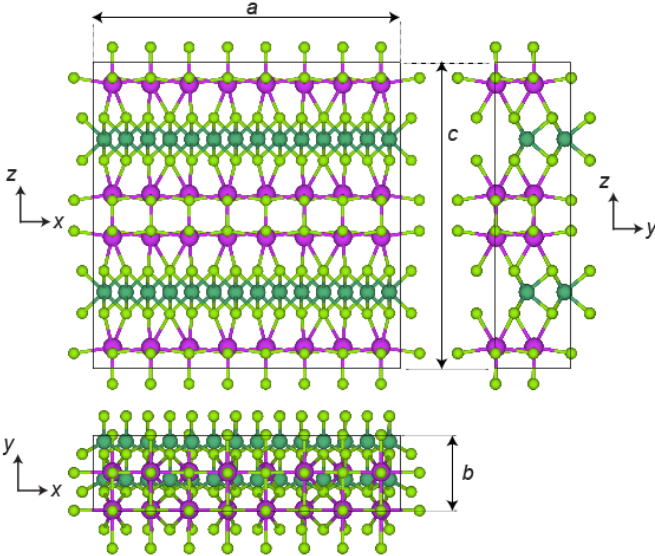


FIG. 8: Approximate commensurate superstructure used for the band structure calculations of the misfit structure. The atoms colors are: Bi: purple, Nb: dark green, Se: light green. The figure was generated using the VESTA package [41].

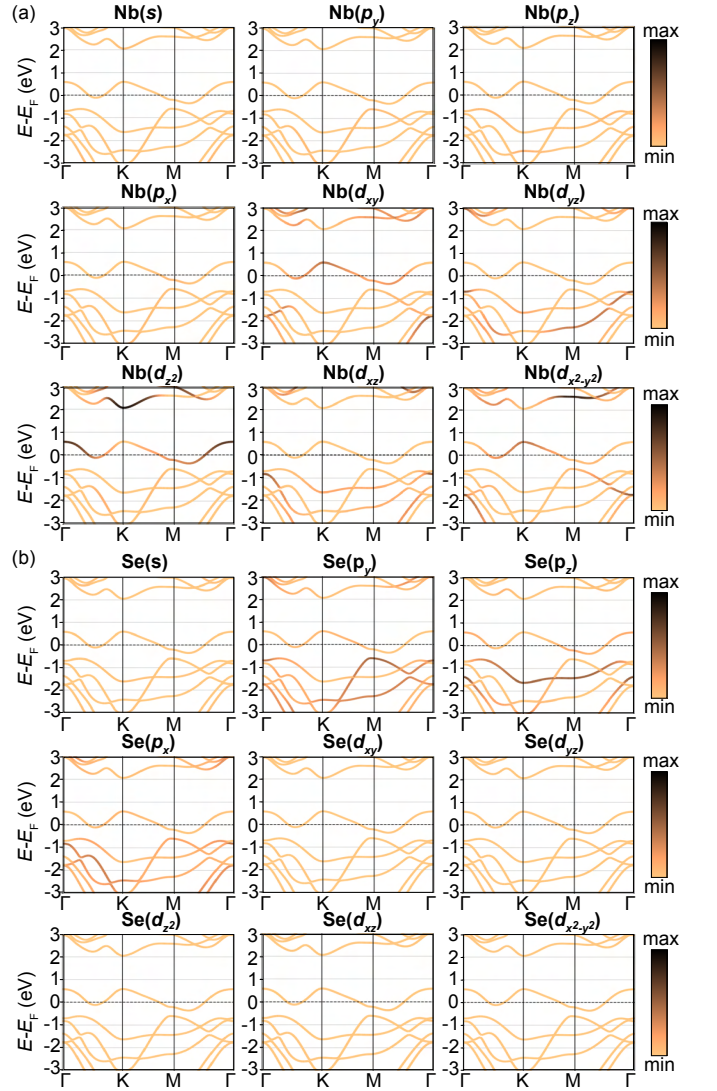


FIG. 9: Band structure and orbital character of single-layer NbSe₂. (a) Nb contribution. (b) Se contribution.

Single-layer band structures and orbital character

The band structures of single-layer NbSe₂ and BiSe are given in Figures 9 and 10, respectively, along with a calculation of the individual bands' orbital character. The single-layer NbSe₂ band structure is in good agreement with previous results [42]. The bands around the Fermi level have dominantly Nb 4d (Bi 6p) character for NbSe₂ (BiSe).

Band unfolding

The unfolded band structures and Fermi contours were computed using the patch version of VASP (Unfolding-Patch4vasp) and the b4vasp package [22], which evaluates the unfolded spectral function defined as follows:

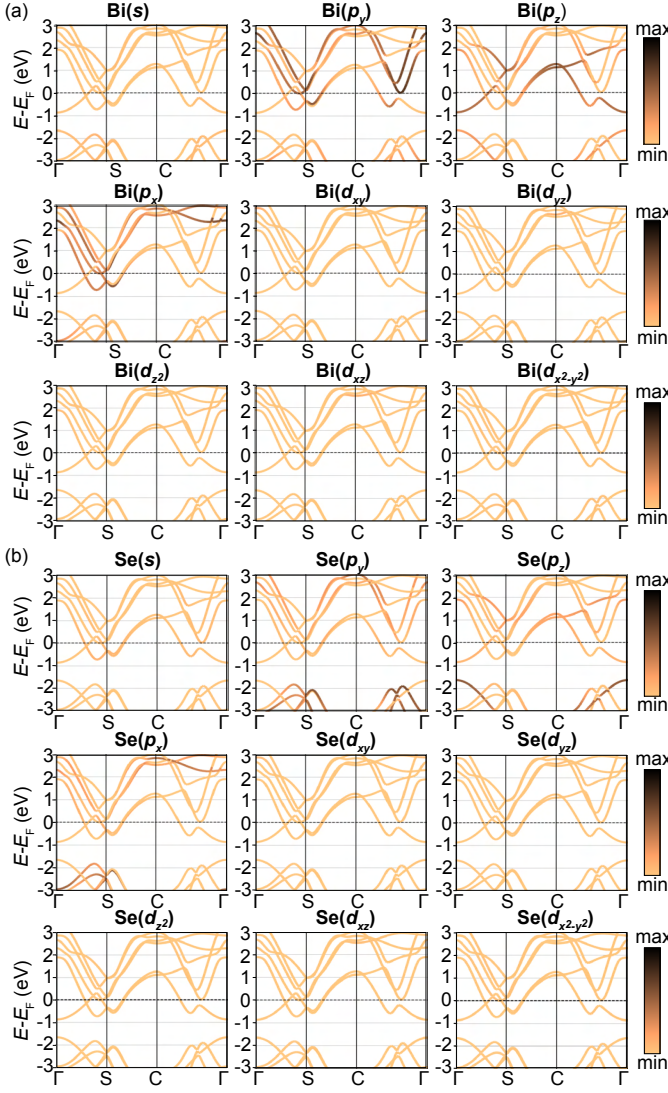


FIG. 10: Band structure and orbital character of single-layer BiSe. (a) Bi contribution. (b) Se contribution.

$$\mathcal{A}(\mathbf{k}, \mathcal{E}) = \sum_{\mathbf{K}m} P_{\mathbf{K}m}(\mathbf{k}) \delta(\mathcal{E} - \mathcal{E}_{\mathbf{K}m}), \quad (1)$$

where \mathcal{E} is the energy, \mathbf{k} is the momentum within the large BZ of the subsystem into which we unfold the band structure, \mathbf{K} is a generic momentum within the misfit mini-BZ, $\mathcal{E}_{\mathbf{K}m}$ are the energies of the misfit Bloch states $|\mathbf{K}, m\rangle$, δ is the Dirac delta function, and

$$P_{\mathbf{K}m}(\mathbf{k}) = \sum_n |\langle \mathbf{k}, n | \mathbf{K}, m \rangle|^2, \quad (2)$$

where the states $|\mathbf{k}, n\rangle$ generate a basis of the Bloch states with momentum \mathbf{k} . Note that $\mathcal{A}(\mathbf{k}, \mathcal{E})$ defined in this way is quite different from the spectral function usually considered in connection with ARPES experiments, which is most often defined based on a single particle dispersion

that is shifted and broadened by the real and imaginary parts of a complex self-energy, respectively [43]. $\mathcal{A}(\mathbf{k}, \mathcal{E})$ should also not be confused with the expected photoemission intensity as neither many-body effects nor photoemission matrix elements are taken into account.

Figure 11 shows the unfolded band structures corresponding to Figure 4 in the main text, i.e., the band structures of single-layer NbSe₂, single-layer BiSe and the misfit approximant unfolded onto the NbSe₂ lattice. In the misfit approximant, several bands from the single-layers remain pronounced: Not surprisingly, the entire NbSe₂ band around the Fermi level can be identified, but also the BiSe electron band around the Γ point is hardly affected by the interlayer interaction. However, half way between the Γ and the K points, the BiSe electron-pocket dispersion shows a substantial redistribution of the spectral weight in the misfit approximant from the single-layer situation, thereby indicating a pronounced interaction between the layers.

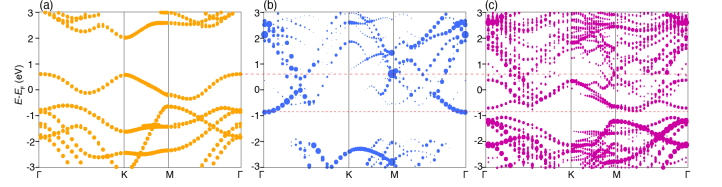


FIG. 11: Band structures unfolded onto the NbSe₂ lattice, corresponding to the Fermi contours in Figure 4(b)-(d) of the main text. (a) Single-layer NbSe₂. (b) Single-layer BiSe. (c) Misfit approximant. The red dashed lines are a guide to the eye for tracking the alignment of the bands in the free-standing layers compared to the misfit structure.

For completeness, in Figure 12 we report the Fermi contours of the individual layers and the misfit approximant, unfolded onto the BZ of the BiSe layers (as opposed to Figure 4 of the main text, where the Fermi contours have been unfolded onto the NbSe₂ lattice). We note that, while one would expect to see results similar to Figure 12 in case of a rigid BiSe lattice dominating the band structure of the NbSe₂ sub-system in the misfit structure, this is not confirmed by the experiments.

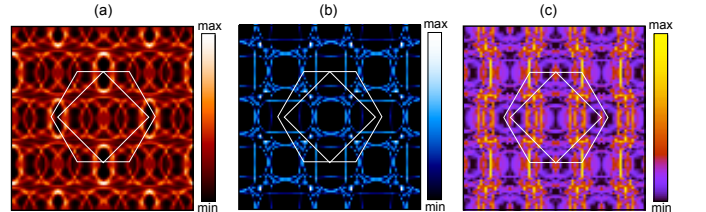


FIG. 12: (a) Spectral function near E_F for NbSe₂ in the approximate unit cell of the misfit structure, unfolded onto the primitive BiSe reciprocal lattice. (b) and (c) Corresponding unfolded spectral function of a free-standing BiSe layer and the complete misfit structure.

Determination of charge transfer

Since the NbSe₂ band structure is still prominently present in the ARPES data from the misfit compound, its band filling can be determined. The increase of filling beyond one electron per unit cell can be interpreted as a charge transfer from the BiSe layers to the NbSe₂ layers under the assumption that there are no other sources of doping (such as charged impurities) in the material. The band filling is determined experimentally by measuring the fraction of the NbSe₂ BZ enclosed by the hole pockets and comparing this to the value of 1/2 for the charge-neutral NbSe₂ layer. The estimated electron doping is 0.26 ± 0.01 additional electrons per Nb-atom. Given the above considerations, this determines just the additional filling of the NbSe₂ band crossing the Fermi energy and not the charge transfer as such because the additional charge could also stem from a doping of the crystal. A conclusive experimental determination of the charge transfer would require the additional determination of the BiSe band filling. This is not possible due to the smeared-out band structure. However, there are some indications supporting a charge transfer. For an overall electron doping of the sample, the BiSe should also be electron doped. However, while we cannot determine the size of the BiSe Fermi contour, comparing the position of the observable electron band at Γ rather suggests that the layer is hole doped, supporting a charge transfer instead. To see this, compare the absolute binding energy of the electron band at Γ in the experiment (≈ 0.4 eV) to the calculated value for free-standing BiSe where it is ≈ 0.7 eV.

A charge transfer within the misfit compound is also supported by the theoretical results. To see this, consider the position of the NbSe₂ hole band and the BiSe electron band at Γ in Figure 11(a) and (b), respectively. Both states remain clearly recognizable in the calculated misfit band structure in Figure 11(c) but with a shift of the NbSe₂ (BiSe) band to lower (higher) energy, supporting the idea of a charge transfer between the layers. Note, however, that the entire concept of a charge transfer becomes problematic in case of appreciable band hybridization, as has been shown for 2D materials interacting with the substrate they have been grown on [44].

* Electronic address: philip@phys.au.dk

- [1] A. K. Geim and I. V. Grigorieva, *Nature* **499**, 419 (2013).
- [2] R. Bistritzer and A. H. MacDonald, *Proceedings of the National Academy of Sciences* **108**, 12233 (2011).
- [3] Y. Cao, V. Fatemi, A. Demir, S. Fang, S. L. Tomarken, J. Y. Luo, J. D. Sanchez-Yamagishi, K. Watanabe, T. Taniguchi, E. Kaxiras, et al., *Nature* **556**, 80 (2018).
- [4] E. Y. Andrei and A. H. MacDonald, *Nature Materials* **19**, 1265 (2020).
- [5] A. J. H. Jones, R. Muzzio, S. Pakdel, D. Biswas, D. Curcio, N. Lanatà, P. Hofmann, K. M. McCreary, B. T. Jonker, K. Watanabe, et al., *2D Materials* **9**, 015032 (2021).
- [6] J. Choi, M. Florian, A. Steinhoff, D. Erben, K. Tran, D. S. Kim, L. Sun, J. Quan, R. Claassen, S. Majumder, et al., *Phys. Rev. Lett.* **126**, 047401 (2021).
- [7] G. Wieggers, *Progress in Solid State Chemistry* **24**, 1 (1996).
- [8] D. Merrill, D. Moore, S. Bauers, M. Falmbigl, and D. Johnson, *Materials* **8**, 2000 (2015).
- [9] G. Wieggers, *Journal of Alloys and Compounds* **219**, 152 (1995).
- [10] Q. Yao, D. W. Shen, C. H. P. Wen, C. Q. Hua, L. Q. Zhang, N. Z. Wang, X. H. Niu, Q. Y. Chen, P. Dudin, Y. H. Lu, et al., *Phys. Rev. Lett.* **120**, 106401 (2018).
- [11] R. T. Leriche, A. Palacio-Morales, M. Campetella, C. Tresca, S. Sasaki, C. Brun, F. Debontridder, P. David, I. Arfaoui, O. Šofranko, et al., *Advanced Functional Materials* **31**, 2007706 (2020).
- [12] S. van Smaalen, *Phys. Rev. B* **43**, 11330 (1991).
- [13] F. Arnold, R.-M. Stan, S. K. Mahatha, H. E. Lund, D. Curcio, M. Dendzik, H. Bana, E. Travaglia, L. Bignardi, P. Lacovig, et al., *2D Materials* **5**, 045009 (2018).
- [14] L. Bignardi, S. K. Mahatha, D. Lizzit, H. Bana, E. Travaglia, P. Lacovig, C. Sanders, A. Baraldi, P. Hofmann, and S. Lizzit, *Nanoscale* **13**, 18789 (2021).
- [15] S. Kraus, F. Huttmann, J. Fischer, T. Knispel, K. Bischof, A. Herman, M. Bianchi, R.-M. Stan, A. J. Holt, V. Caciuc, et al., *Phys. Rev. B* **105**, 165405 (2022).
- [16] W. Zhou, A. Meetsma, J. de Boer, and G. Wieggers, *Materials Research Bulletin* **27**, 563 (1992).
- [17] A. Nader, A. Briggs, and Y. Gotoh, *Solid State Communications* **101**, 149 (1997).
- [18] M. Nagao, A. Miura, Y. Horibe, Y. Maruyama, S. Watauchi, Y. Takano, and I. Tanaka, *Solid State Communications* **321**, 114051 (2020).
- [19] S. V. Hoffmann, C. Søndergaard, C. Schultz, Z. Li, and P. Hofmann, *Nuclear Instruments and Methods in Physics Research, A* **523**, 441 (2004).
- [20] G. Kresse and J. Furthmüller, *Computational Materials Science* **6**, 15 (1996).
- [21] G. Kresse and D. Joubert, *Physical Review B* **59**, 1758 (1999).
- [22] D. Dirnberger, G. Kresse, C. Franchini, and M. Reticcioli, *Journal of Physical Chemistry C* **125**, 12921 (2021).
- [23] S. V. Borisenko, A. A. Kordyuk, V. B. Zabolotnyy, D. S. Inosov, D. Evtushinsky, B. Büchner, A. N. Yaresko, A. Varykhalov, R. Follath, W. Eberhardt, et al., *Phys. Rev. Lett.* **102**, 166402 (2009).
- [24] D. J. Rahn, S. Hellmann, M. Kalläne, C. Sohrt, T. K. Kim, L. Kipp, and K. Rossnagel, *Phys. Rev. B* **85**, 224532 (2012).
- [25] F. Weber, R. Hott, R. Heid, L. L. Lev, M. Caputo, T. Schmitt, and V. N. Strocov, *Phys. Rev. B* **97**, 235122 (2018).
- [26] Y. Nakata, K. Sugawara, S. Ichinokura, Y. Okada, T. Hitosugi, T. Koretsune, K. Ueno, S. Hasegawa, T. Takahashi, and T. Sato, *npj 2D Materials and Applications* **2**, 12 (2018).
- [27] C.-Z. Xu, X. Wang, P. Chen, D. Flötotto, J. A. Hlevyack, M.-K. Lin, G. Bian, S.-K. Mo, and T.-C. Chiang, *Phys. Rev. Materials* **2**, 064002 (2018).
- [28] P. Dreher, W. Wan, A. Chikina, M. Bianchi, H. Guo,

- R. Harsh, S. Mañas-Valero, E. Coronado, A. J. Martínez-Galera, P. Hofmann, et al., *ACS Nano* (2021).
- [29] E. Kabliman, P. Blaha, and K. Schwarz, *Phys. Rev. B* **82**, 125308 (2010).
- [30] M. Grioni, S. Pons, and E. Frantzeskakis, *Journal of Physics: Condensed Matter* **21**, 023201 (2008).
- [31] S. van Smaalen, *Journal of Physics: Condensed Matter* **3**, 1247 (1991).
- [32] V. Petříček, I. Cisarova, J. L. de Boer, W. Zhou, A. Meetsma, G. A. Wiegers, and S. van Smaalen, *Acta Crystallographica Section B Structural Science* **49**, 258 (1993).
- [33] Y. Nakata, K. Sugawara, S. Ichinokura, Y. Okada, T. Hitosugi, T. Koretsune, K. Ueno, S. Hasegawa, T. Takahashi, and T. Sato, *npj 2D Materials and Applications* **2** (2018).
- [34] G. Mitchson, M. Falmbigl, J. Ditto, and D. C. Johnson, *Inorganic Chemistry* **54**, 10309 (2015).
- [35] K. Suzuki, T. Kondo, T. Enoki, and S. Bandow, *Synthetic Metals* **56**, 1741 (1993).
- [36] S. Aubry and G. André, *Ann. Israel Phys. Soc* **3**, 18 (1980).
- [37] M. Kohmoto, *Phys. Rev. Lett.* **51**, 1198 (1983).
- [38] J. P. Perdew, K. Burke, and M. Ernzerhof, *Physical Review B* **77**, 3865 (1996).
- [39] J. P. Perdew, J. A. Chevary, S. H. Vosko, K. A. Jackson, M. R. Pederson, D. J. Singh, and C. Fiolhais, *Physical Review B* **46**, 6671 (1992).
- [40] S. Grimme, J. Antony, S. Ehrlich, and H. Krieg, *Journal of Chemical Physics* **132**, 154104 (2010).
- [41] K. Momma and F. Izumi, *Journal of Applied Crystallography* **44**, 1272 (2011).
- [42] M. Calandra, I. I. Mazin, and F. Mauri, *Phys. Rev. B* **80**, 241108 (2009).
- [43] P. Hofmann, I. Y. Sklyadneva, E. D. L. Rienks, and E. V. Chulkov, *New Journal of Physics* **11**, 125005 (2009).
- [44] B. Shao, A. Eich, C. Sanders, A. S. Nganheu, M. Bianchi, P. Hofmann, A. A. Khajetoorians, and T. O. Wehling, *Nature Communications* **10**, 180 (2019).